LETTER

doi:10.1038/nature10907

Wild-type microglia arrest pathology in a mouse model of Rett syndrome

Noël C. Derecki[1,2], James C. Cronk[1,2,3], Zhenjie Lu[1], Eric Xu[1,4], Stephen B. G. Abbott[5], Patrice G. Guyenet[5] & Jonathan Kipnis[1,2,3]

Rett syndrome is an X-linked autism spectrum disorder. The disease is characterized in most cases by mutation of the *MECP2* gene, which encodes a methyl-CpG-binding protein[1–5]. Although MECP2 is expressed in many tissues, the disease is generally attributed to a primary neuronal dysfunction[6]. However, as shown recently, glia, specifically astrocytes, also contribute to Rett pathophysiology. Here we examine the role of another form of glia, microglia, in a murine model of Rett syndrome. Transplantation of wild-type bone marrow into irradiation-conditioned *Mecp2*-null hosts resulted in engraftment of brain parenchyma by bone-marrow-derived myeloid cells of microglial phenotype, and arrest of disease development. However, when cranial irradiation was blocked by lead shield, and microglial engraftment was prevented, disease was not arrested. Similarly, targeted expression of MECP2 in myeloid cells, driven by *Lysm*^{cre} on an *Mecp2*-null background, markedly attenuated disease symptoms. Thus, through multiple approaches, wild-type *Mecp2*-expressing microglia within the context of an *Mecp2*-null male mouse arrested numerous facets of disease pathology: lifespan was increased, breathing patterns were normalized, apnoeas were reduced, body weight was increased to near that of wild type, and locomotor activity was improved. *Mecp2*$^{+/-}$ females also showed significant improvements as a result of wild-type microglial engraftment. These benefits mediated by wild-type microglia, however, were diminished when phagocytic activity was inhibited pharmacologically by using annexin V to block phosphatydilserine residues on apoptotic targets, thus preventing recognition and engulfment by tissue-resident phagocytes. These results suggest the importance of microglial phagocytic activity in Rett syndrome. Our data implicate microglia as major players in the pathophysiology of this devastating disorder, and suggest that bone marrow transplantation might offer a feasible therapeutic approach for it.

The role of glia in Rett syndrome has recently been recognized[7–9]. *Mecp2*-null astrocytes were unable to support the normal dendritic ramification of wild-type neurons growing in culture[7], and expression of wild-type MECP2 protein in astrocytes of *Mecp2*-null hosts dramatically ameliorated disease pathology[9]. *Mecp2*-null microglia were reported to be toxic to neurons *in vitro* through production of high levels of glutamate[10].

Microglia, the brain-resident macrophages, are of haematopoietic origin[11]. Still, the idea of repopulation of brain microglia from bone-marrow-derived cells in adult mice under normal physiological conditions is controversial[12]. However, when bone marrow transplantation is preceded by irradiation-mediated immune ablation, bone-marrow-derived cells with microglia-like morphology and phenotype (expressing low levels of CD45 and high levels of CD11b) are found in the brain[13,14]. Microglia have received increasing attention in the pathophysiology of several neurodegenerative and neuropsychiatric diseases[14–18].

We first studied microglial function in the context of *Mecp2*$^{-/y}$ male mice. Males possess a single mutant X chromosome, and thus manifest a severe phenotype that includes markedly retarded growth, apnoeas, tremor, impaired gait and locomotor function, and a postnatal life expectancy of approximately 8 weeks[4,19] (Fig. 1a, b and Supplementary Movie 1).

To address the role of hematopoietically derived cells in the pathophysiology of Rett, *Mecp2*$^{-/y}$ (*Mecp2*$^{tm1.1Jae}$ and *Mecp2*^{tm2Bird}) mice were subjected to lethal split-dose irradiation at postnatal day (P)28 (the approximate age at which neurological signs appear[4]). Mice were then injected intravenously with syngeneic bone marrow from C57Bl/6J mice ubiquitously expressing green fluorescent protein (GFP). Control groups were injected with autologous (*Mecp2*$^{-/y}$) bone marrow, or left naive. Surprisingly, the lifespan of *Mecp2*-null recipients of wild-type bone marrow (wild type → *Mecp2*$^{-/y}$) was significantly extended compared with *Mecp2*$^{-/y}$ mice receiving autologous bone marrow (*Mecp2*$^{-/y}$ → *Mecp2*$^{-/y}$) or to naive *Mecp2*$^{-/y}$ mice (Fig. 1b and Supplementary Movie 2). Our oldest living wild-type → *Mecp2*$^{-/y}$ mice were over 48 weeks of age (Supplementary Movie 3); most experimental mice were euthanized at the age of ~16 weeks for tissue analysis.

Although *Mecp2*$^{-/y}$ mice on the C57Bl/6J background are undersized[4,19], within 4 weeks of transplantation, wild-type → *Mecp2*$^{-/y}$ (but not *Mecp2*$^{-/y}$ → *Mecp2*$^{-/y}$) mice approached the size of wild-type littermates (Fig. 1c, d). Wild-type → *Mecp2*$^{-/y}$ mice also exhibited an increase in brain weight (Fig. 1e, f), which was probably caused by general growth of the mouse, because the reduced soma size characteristic of *Mecp2*-null neurons was not changed by bone marrow transplantation (Fig. 1g, h) and the brain to body weight ratio was normalized (Supplementary Fig. 1a). Spleens of *Mecp2*$^{-/y}$ mice were also smaller than normal and their size normalized after transplantation (Supplementary Fig. 1b–d).

Growth retardation is a characteristic feature of Rett pathology. Along these lines, treatment with insulin-like growth factor (IGF)-1 benefits survival and behavioural outcomes in *Mecp2*-null mice[20]. Indeed, peripheral macrophages from wild-type mice expressed significantly higher levels of IGF-1 *in vitro* in response to immunological stimuli than macrophages from *Mecp2*-null (*Mecp2*$^{tm1.1Jae/y}$) mice (Supplementary Fig. 2); this difference may contribute to the increased body growth seen in *Mecp2*-null mice after bone marrow transplantation.

The general appearance of wild-type → *Mecp2*$^{-/y}$ mice was improved compared with that of naive *Mecp2*$^{-/y}$ or *Mecp2*$^{-/y}$ → *Mecp2*$^{-/y}$ mice. The severe involuntary tremors normally seen in mutant mice were absent following wild-type bone marrow transplantation (Fig. 2a), and gait was improved. Interestingly, no detectable benefit on hindlimb clasping phenotype was observed.

Breathing irregularities and apnoeas are cardinal signs of Rett syndrome. We used whole-body plethysmography to compare the breathing patterns of *Mecp2*$^{-/y}$ mice with or without bone marrow transplantation to those of control mice (Fig. 2b). As expected, *Mecp2*$^{-/y}$ mice developed apnoeas progressively with age (data not shown). However, wild type → *Mecp2*$^{-/y}$ exhibited significantly reduced apnoeas and fewer breathing irregularities than either naive *Mecp2*$^{-/y}$ or

[1]Department of Neuroscience, School of Medicine, University of Virginia, Charlottesville, Virginia 22908, USA. [2]Graduate Program in Neuroscience, School of Medicine, University of Virginia, Charlottesville, Virginia 22908, USA. [3]Medical Scientist Training Program, School of Medicine, University of Virginia, Charlottesville, Virginia 22908, USA. [4]Undergraduate School of Arts and Sciences, University of Virginia, Charlottesville, Virginia 22908, USA. [5]Department of Pharmacology, School of Medicine, University of Virginia, Charlottesville, Virginia 22908, USA.

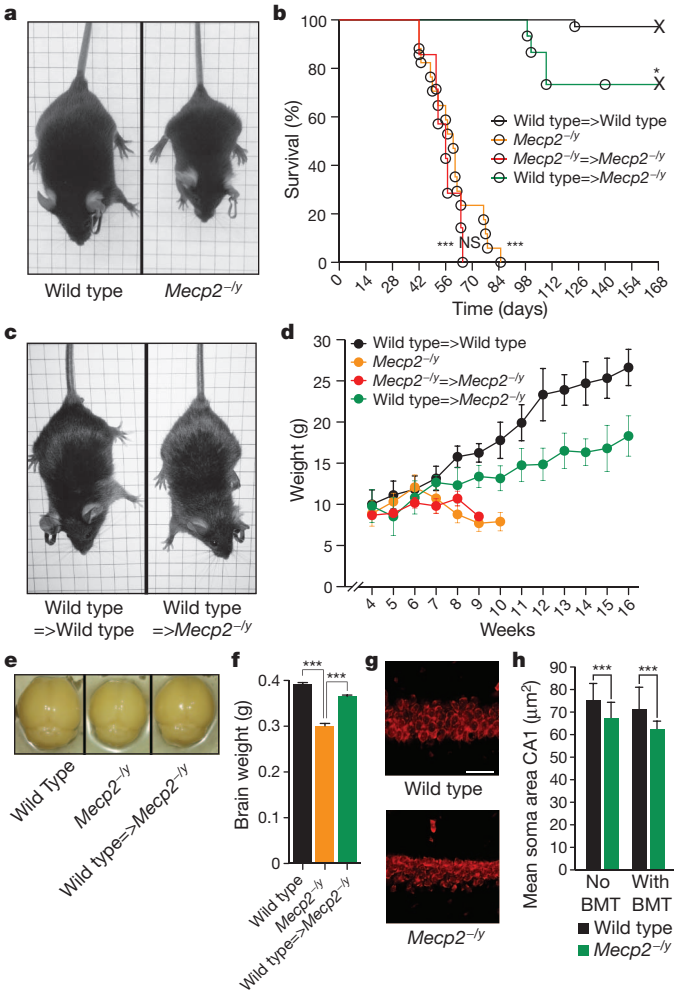

Figure 1 | Wild-type bone marrow transplantation (BMT) at P28 arrests disease progression in *Mecp2*$^{-/y}$ mice. **a**, Representative images of wild-type and *Mecp2*$^{-/y}$ littermates at P56. **b**, Lifespan of *Mecp2*$^{-/y}$ mice receiving wild-type bone marrow at P28 (wild type → *Mecp2*$^{-/y}$; $n = 15$) compared with naive *Mecp2*$^{-/y}$ ($n = 17$), *Mecp2*$^{-/y}$ receiving *Mecp2*$^{-/y}$ bone marrow (*Mecp2*$^{-/y}$ → *Mecp2*$^{-/y}$; $n = 9$) and wild-type mice receiving wild-type bone marrow (wild type → wild type; $n = 29$) (***$P < 0.0001$, log rank (Mantel–Cox)). **c**, Representative images of wild-type → wild-type compared with wild-type → *Mecp2*$^{-/y}$ mice are shown at P56 (4 weeks after bone marrow transplantation). **d**, Weights (mean ± s.e.m.) of wild-type → wild-type, *Mecp2*$^{-/y}$, *Mecp2*$^{-/y}$ → *Mecp2*$^{-/y}$ and wild-type → *Mecp2*$^{-/y}$ mice ($n = 15, 15, 7, 15$ mice per group) are shown over time. **e**, Representative images of brains isolated from P56 wild-type → wild-type and wild-type → *Mecp2*$^{-/y}$ mice transplanted at P28 and naive *Mecp2*$^{-/y}$ mice. **f**, Brain weight (mean ± s.e.m.) for each group (***$P < 0.001$; one-way analysis of variance (ANOVA); $n = 4$ each group). **g**, Representative images of Nissl staining in hippocampal slices (CA1 area) of wild-type and *Mecp2*$^{-/y}$ mice (scale bar, 40 μm). **h**, Soma area (mean ± s.d.) of CA1 hippocampal cells. For each group of mice, a set of cells was created by randomly selecting 100 cells per mouse, three mice per group (***$P < 0.001$; two-way ANOVA with Bonferroni *post hoc* test).

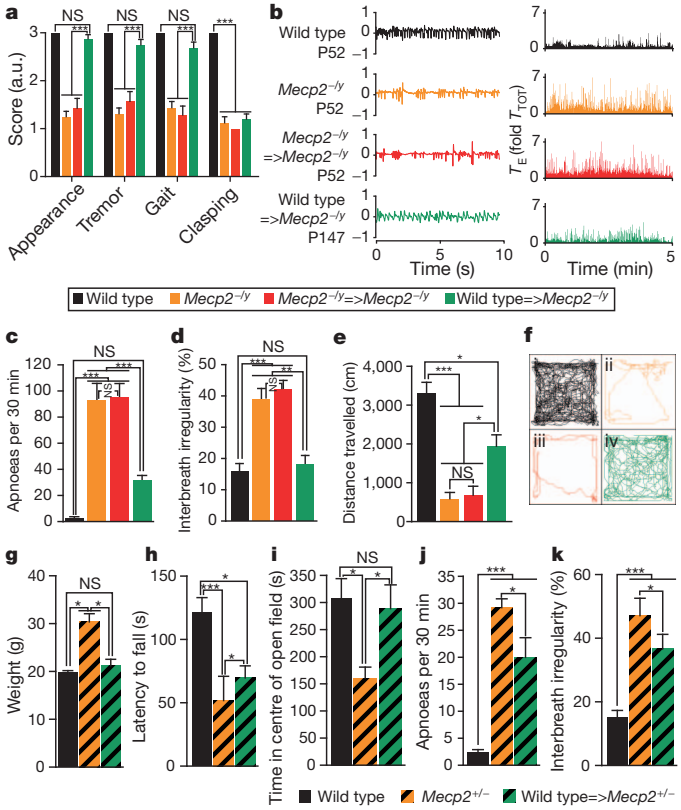

Figure 2 | Bone marrow transplantation effects on general appearance, breathing and locomotion of *Mecp2*$^{-/y}$ and *Mecp2*$^{+/-}$ mice. **a**, Neurological scores at P56 for wild-type → wild-type, *Mecp2*$^{-/y}$ naive, *Mecp2*$^{-/y}$ → *Mecp2*$^{-/y}$ and wild-type → *Mecp2*$^{-/y}$ mice. Behaviours (mean ± s.e.m.) are scored as indicated in Methods (***$P < 0.001$; one-way ANOVA; $n = 16, 16, 7, 16$); NS, not significant; a.u., arbitrary units. **b**, Left, representative plethysmograph recordings of animals from each group; right, expiratory time (T_E) for representative wild-type, *Mecp2*$^{-/y}$, *Mecp2*$^{-/y}$ → *Mecp2*$^{-/y}$ and wild-type → *Mecp2*$^{-/y}$ mice (transplantation at P28 and examination at indicated ages for all groups) as measured over 5 min; T_E is normalized to mean breath duration for each mouse. **c**, Apneas (mean ± s.e.m.) per 30 min as measured in all four groups (***$P < 0.001$; one-way ANOVA with Bonferroni *post hoc* test; $n = 5$ mice per group; for the entire figure, all mice were age P56 except for wild type → *Mecp2*$^{-/y}$ at 12 weeks of age; that is, 8 weeks after bone marrow transplantation). **d**, Interbreath irregularity (mean percentage ± s.e.m.) calculated as absolute $((T_{total,n} - T_{total,n+1})/T_{total,n+1})$ for all four groups (**$P < 0.01$; ***$P < 0.001$; one-way ANOVA with Bonferroni *post hoc* test; $n = 5$ mice per group). **e**, Distance travelled (mean ± s.e.m.) in an open field (*$P < 0.05$; ***$P < 0.001$; one-way ANOVA, $n = 5$ mice per group). **f**, Representative traces of the path travelled by mice in an open field during 20 min test time. **g**–**k**, *Mecp2*$^{+/-}$ mice were transplanted with wild-type bone marrow at P56 and were examined for disease symptoms at 9 months of age. **g**, Weight (mean ± s.e.m.); **h**, latency to fall (mean ± s.e.m.) in the rotarod task; **i**, time (mean ± s.e.m.) spent in the centre of the open field; **j**, apneas (mean ± s.e.m.) measured by whole-body plethysmography in 30 min; **k**, interbreath irregularity (mean % ± s.e.m.): all were improved in the treated mice compared with non-treated controls (*$P < 0.05$; ***$P < 0.001$; one-way ANOVA, $n = 6$ mice per group; *post hoc* Bonferroni test was used for individual comparisons).

Mecp2$^{-/y}$ → *Mecp2*$^{-/y}$ mice (Fig. 2c, d). Wild-type → *Mecp2*$^{-/y}$ mice also displayed significantly increased mobility in the open field compared with naive *Mecp2*$^{-/y}$ or *Mecp2*$^{-/y}$ → *Mecp2*$^{-/y}$ mice (Fig. 2e, f).

We also performed bone marrow transplantation in heterozygous female mice at 2 months of age, and animals were examined at 9 months. The disease in *Mecp2*$^{+/-}$ mice develops slowly, with behavioural abnormalities becoming clear at 4–6 months of age. Weights of treated *Mecp2*$^{+/-}$ mice were comparable to wild-type controls (Fig. 2g). Moreover, there was significant improvement in motor function, as examined on rotarod (Fig. 2h), and time spent in the centre of the open field arena was significantly increased (Fig. 2i). Apnoeas in bone marrow transplanted mice were reduced (Fig. 2j) and their overall breathing patterns were improved compared with their non-treated controls (Fig. 2k).

The peripheral immune system of *Mecp2*$^{-/y}$ hosts was repopulated by donor bone marrow (Supplementary Fig. 3a). Additionally, it has been previously shown that bone marrow transplantation after whole-body irradiation results in engraftment of microglia-like myeloid cells into the brain parenchyma[13]. Indeed, GFP^{+} cells in the parenchyma of bone marrow transplanted mice expressed CD11b (Fig. 3a) but not GFAP or NeuN (data not shown). Twelve weeks after bone marrow transplantation, mice were perfused and their brains dissected into

sub-areas, prepared in single-cell suspensions and analysed using flow cytometry to determine percentages of bone-marrow-derived (GFP^+) cells in the haematopoietic ($CD45^+$) cell fractions in the brain (Supplementary Fig. 3b, c).

Interestingly, in mice in which bone marrow transplantation was performed later (P40 or P45), only slight improvements in disease pathology were observed (Supplementary Fig. 4a). No microglial engraftment was evident, although substantial numbers of GFP^+ cells were found in the meningeal spaces (Supplementary Fig. 4b). These results may suggest that when disease progression is faster than microglial engraftment, full rescue cannot be achieved. The moderate results observed, however, may have been due to a yet-unknown mechanism, perhaps through soluble factors produced by meningeal immune cells, or peripherally-expressed IGF-1 (Supplementary Fig. 2). When bone marrow transplantation was performed at P2 without irradiation, minimal peripheral chimaerism was achieved without detectable microglial engraftment and no lifespan extension was observed (Supplementary Fig. 4a, c).

Newly engrafted microglia expressed detectable levels of wild-type *Mecp2* (data not shown) but nearby cells did not show any *Mecp2* labelling, arguing against the possibility of protein or messenger RNA transfer from engrafted microglia into nearby cells as an underlying mechanism for the beneficial effect of bone marrow transplantation.

To substantiate the specific role of microglia in bone marrow transplantation-mediated disease arrest, we repeated transplantation experiments, again at P28, but with the addition of lead shielding to block cranial irradiation, which results in repopulation of peripheral immunity (Fig. 3b, c) but no parenchymal engraftment (Fig. 3d), supporting previously published work[13,18]. Disease was not arrested in 'head-covered' mice (Fig. 3e), suggesting that peripheral immune reconstitution without microglial engraftment is insufficient to arrest pathology in $Mecp2^{-/y}$ mice.

To substantiate further the role of myeloid cells in arrest of Rett pathology, we used a genetic approach. We employed the widely used $Lysm^{Cre}$ mouse—which results in a high degree of recombination in myeloid cells, granulocytes and in significant numbers of microglia[21–23]—in cross with $Mecp2^{lox-stop}$ mice. Male progeny, $Mecp2^{lox-stop/y}Lysm^{cre}$, express wild-type *Mecp2* in myeloid cells on an otherwise *Mecp2*-null background. These animals exhibited improvements in overall appearance and growth (Fig. 3f, g and Supplementary Movie 4) and their lifespans were significantly increased (Fig. 3h). The oldest $Mecp2^{lox-stop/y}Lysm^{cre}$ animals were 31 weeks of age, with survival of 100%; $n = 6$ mice per group. Apnoeas and interbreath irregularity of these mice were also significantly reduced compared with control mice (Fig. 3i, j), and their open field activity was not significantly different from wild-type counterparts (Fig. 3k). These results cannot be interpreted by cre leakiness, because no cre-mediated recombination was evident in either astrocytes or neurons in $Lysm^{cre}$ crossed to a reporter strain (data not shown), in line with previous publications[22,23].

Microglia from *Mecp2*-null mice were deficient in their response to immunological stimuli (Supplementary Fig. 5) and in phagocytic capacity, as examined by feeding cultured microglia with pre-labelled ultraviolet-irradiated neural progenitor cells, used as apoptotic targets[24] (Fig. 4a–c). Thus, it is possible that apoptotic debris would accumulate over time in the *Mecp2*-null brain, contributing to neuronal malfunction and accelerating disease progression. Along these lines, supplementation of wild-type microglia could reduce debris levels and allow improved neuronal function. Indeed, in mice transplanted with GFP^+

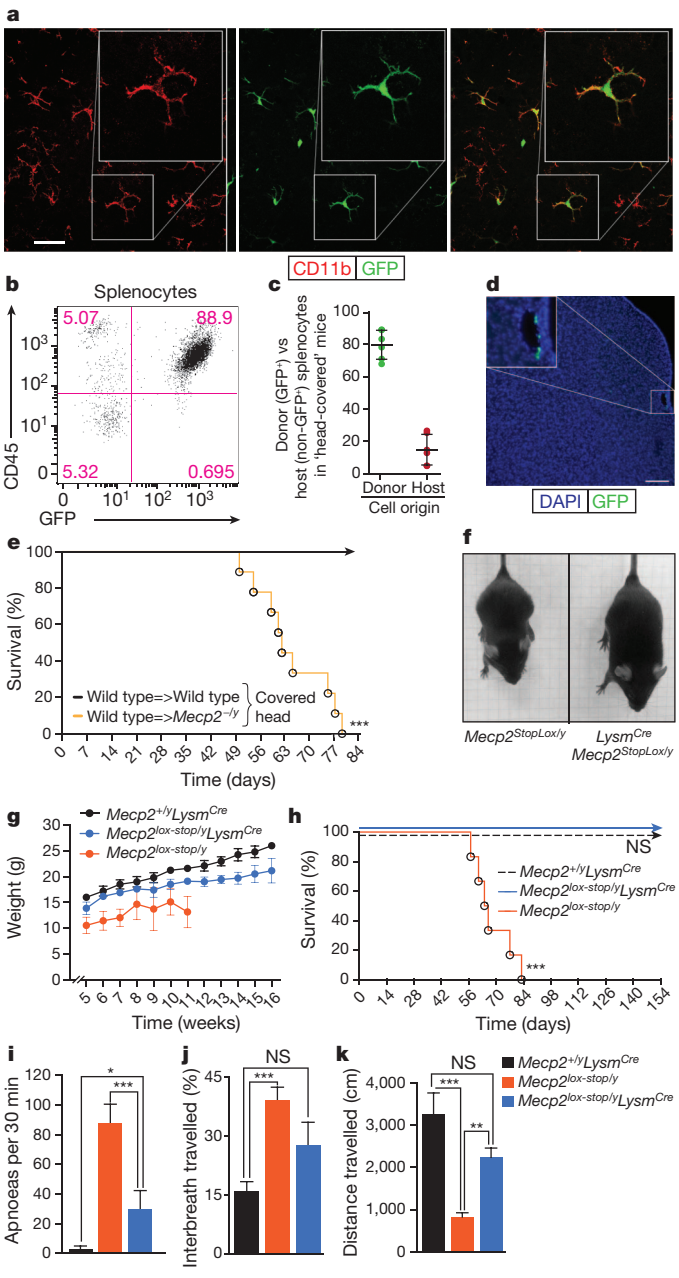

Figure 3 | Brain parenchymal engraftment of cells after bone marrow transplantation is required to arrest Rett syndrome. **a**, Representative confocal images of brain parenchyma from cerebellum of wild-type → $Mecp2^{-/y}$ mice 8 weeks after transplantation (at P28), immunolabelled for CD11b and GFP (scale bar, 20 μm). **b**–**e**, $Mecp2^{-/y}$ mice underwent bone marrow transplantation at P28 with their heads lead-protected. Mice were examined at their end-point, about 7 weeks after bone marrow transplantation. **b**, Representative dot plot of splenocytes obtained from bone-marrow-transplanted mouse with lead-protected head. **c**, Distribution of 'peripheral chimaerism' in mice with lead-protected heads after bone marrow transplantation. **d**, Representative micrograph from mice with lead-protected heads after bone marrow transplantation, immunolabelled for GFP. Coronal cortical slice is presented showing sporadic cells found in meningeal spaces, but not in the parenchyma. **e**, Lifespan of $Mecp2^{-/y}$ mice with wild-type bone marrow transplantation with lead-covered heads compared with wild-type → wild-type controls with lead-covered heads (***$P < 0.0001$, log rank (Mantel–Cox); $n = 9$ mice per group). **f**–**k**, Genetic approach for expressing MECP2 protein in myeloid cells. $Mecp2^{lox-stop}$ mice were bred to $Lysm^{Cre}$ mice and their progeny ($Mecp2^{lox-stop/y}Lysm^{Cre}$ mice) were analysed for disease progression. **f**, Representative image of mice at P56. **g**, Weights (mean ± s.e.m.) of mice as they progress with age. **h**, Lifespan for indicated groups (***$P < 0.0001$, log rank (Mantel–Cox); $n = 6$ mice per group). **i**, Apnoeas (mean ± s.e.m.) measured by whole-body plethysmography in 30 min for the three groups at 9 weeks. **j**, Interbreath irregularity (mean % ± s.e.m.) measured at 9 weeks. **k**, Distance travelled (mean ± s.e.m.) in an open field at 9 weeks (**$P < 0.01$; ***$P < 0.001$; one-way ANOVA, $n = 5$ mice per group; Bonferroni *post hoc* test was used for individual comparisons).

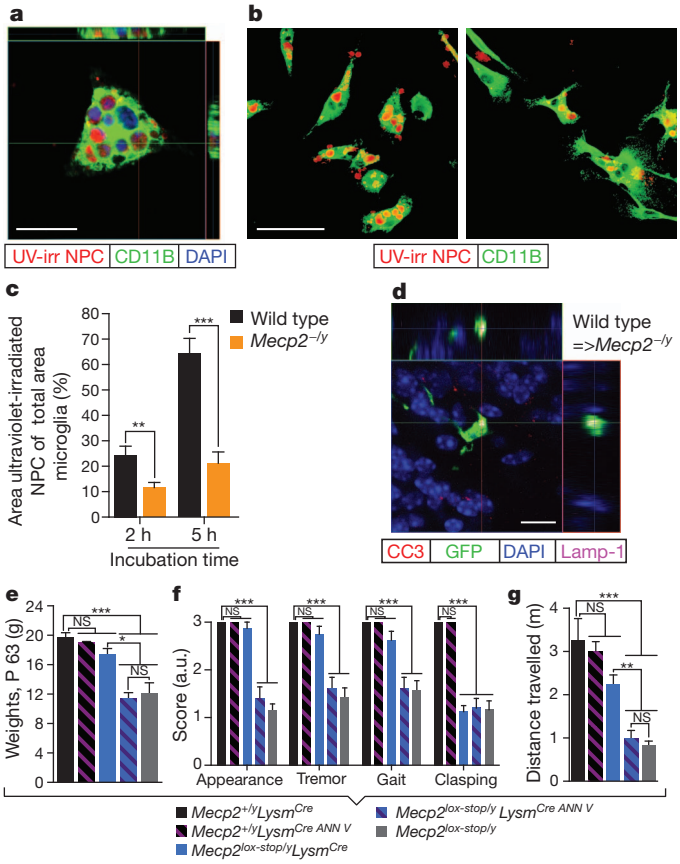

Figure 4 | Microglial phagocytic activity is necessary for their beneficial effect in *Mecp2*$^{-/y}$ mouse brains. **a**, Representative micrograph of phagocytosing microglia in orthogonal projections of confocal z-stacks. Scale bar, 25 μm. **b**, Wild-type (left) or *Mecp2*$^{-/y}$ (right) microglia incubated for 2 or 5 h with fluorescently labelled ultraviolet-irradiated neural progenitor cells and stained with anti-CD11b. Scale bar, 50 μm. **c**, Bar graphs comparing surface area of ultraviolet-irradiated neural progenitor cells (NPC) to total surface area (mean ± s.e.m.) of wild-type or *Mecp2*$^{-/y}$ microglia (**$P < 0.01$; ***$P < 0.001$; one-way ANOVA; representative experiment shown out of three independently performed). **d**, Representative micrograph of phagocytosing microglia *in situ* containing cleaved caspase-3 debris co-localized with lysosomal marker, Lamp-1. Scale bar, 50 μm. **e**–**g**, *Mecp2*$^{lox-stop/y}$*Lysm*^{Cre} mice and the appropriate controls were treated with annexin V to inhibit phagocytic activity pharmacologically. **e**, Weights (mean ± s.e.m.) of *Mecp2*$^{+/y}$*Lysm*^{Cre}, *Mecp2*$^{lox-stop/y}$*Lysm*^{Cre}, *Mecp2*$^{lox-stop/y}$, *Mecp2*$^{+/y}$*Lysm*^{Cre} mice treated with annexin V and *Mecp2*$^{lox-stop/y}$*Lysm*^{Cre} mice treated with annexin V are shown at the end point for *Mecp2*$^{lox-stop/y}$ and *Mecp2*$^{lox-stop/y}$*Lysm*^{Cre} treated with annexin V groups (~P63). **f**, Neurological scores (mean ± s.e.m.) at P56 are presented (***$P < 0.001$; one-way ANOVA; n = at least seven mice per group; Bonferroni *post hoc* test was used for individual comparisons). **g**, Distance travelled (mean ± s.e.m.) in an open field by mice from all the above groups (***$P < 0.001$; one-way ANOVA, $n = 5$ mice per group; Bonferroni *post hoc* test was used for individual comparisons).

bone marrow, only GFP$^+$ parenchymal cells were consistently found containing cleaved caspase-3-positive debris within lysosomes (Fig. 4d).

It has been previously shown that annexin V (a protein that binds phosphatidylserine on apoptotic cells and inhibits engulfment) injected intravenously can reach the central nervous system[25]. Moreover, we have recently shown that intravenous injection of annexin V results in substantial blockade of phagocytic activity in the brain[24]. Indeed, treatment of wild-type mice with annexin V resulted in significant accumulation of terminal deoxynucleotidyl transferase (TdT)-mediated dUTP nick end labelling (TUNEL)$^+$ fragments (Supplementary Fig. 6).

We attempted to inhibit brain phagocyte activity pharmacologically in *Mecp2*$^{lox-stop/y}$*Lysm*^{cre} mice and compare disease progression with controls. Long-term treatment of *Mecp2*$^{lox-stop/y}$*Lysm*^{cre} mice with annexin V abolished the amelioration of the disease normally seen in these mice (Fig. 4e–g). Wild-type mice treated with annexin V were not significantly affected. This is probably because, unlike in *Mecp2*$^{lox-stop/y}$*Lysm*^{cre} mice, neurons and astrocytes in wild-type mice are fully functional, expressing wild-type MECP2. It is conceivable, however, that a longer treatment of wild-type mice with annexin V might result in neurological pathology. Overall, these results suggest active engagement of wild-type microglia in clearance of apoptotic cells or cell remnants within the context of otherwise *Mecp2*-null brain—a task that probably cannot be sufficiently performed by *Mecp2*-null microglia.

Neuropathologists have observed gliosis and cell loss in the cerebellum of deceased patients who had Rett syndrome [26], but this work has not received much attention, presumably because the disease is generally considered non-neurodegenerative. Our results do not claim that neurodegeneration underlies the pathology of the disease. Rather, they suggest that *Mecp2*-null microglia, deficient in phagocytic function, may be unable to keep pace in clearing debris left behind from the normal process of neural cell death or membrane shedding. This, in turn, would lead to a crowded and sub-optimal central nervous system milieu within which neurons, already challenged by loss of *Mecp2*, might be further impaired in function. The inability of *Mecp2*-null microglia to clear debris as effectively as wild-type microglia has the potential to contribute to the underlying neuropathology and/or the time course of appearance of symptoms in *Mecp2*-null mice[4,27].

Future studies should be aimed at understanding the connections between glial phagocytic activity and neuronal function, and possible interactions between microglia and astrocytes in the pathology of Rett syndrome. Phagocytic activity per se is almost certainly just one aspect of glial involvement in the pathophysiology of the disease. It is conceivable that glia, including astrocytes—which are also capable phagocytes[28]—release soluble factors in connection with their own phagocytic activity, in turn benefiting neuronal function. Therefore, removal of debris itself may not be as primarily relevant to disease progression as a secondary response of glia to the phagocytic process. Accordingly, inhibition of phagocytosis might result in exacerbation of pathology of the disease through these as yet unknown processes, even in the absence of deposits of easily observable cellular debris.

Our present findings support previous publications describing the potential for clinical treatment of Rett pathology[6,29], while also suggesting the possibility of achieving this goal through augmentation or repopulation of brain phagocytes, or improvement of their phagocytic activity. These results open the possibility for a new approach in the amelioration of the pathology of Rett syndrome.

METHODS SUMMARY

Animals. Male and female C57Bl/6-Tg(UBC-GFP)30Scha/J, C57Bl/6J, B6.129P2(C)Mecp2$^{tm1.1Bird}$/J, B6.129P2-Lyz2$^{tm1(cre)Ifo}$/J (*Lysm*^{cre}), B6.129P2-Mecp2^{tm2Bird}/J, *Mecp2*$^{lox-stop/y}$ and C57BL/6J mice were purchased from Jackson Laboratories; B6.Cg-Mecp2$^{tm1.1Jae/Mmcd}$ mice were a gift from A. Pieper and maintained in our laboratory on C57Bl/6J background. All procedures complied with regulations of the Institutional Animal Care and Use Committee at The University of Virginia.

Irradiation and bone marrow transfer. Four-week-old mice were subjected to lethal split-dose γ-irradiation (300 rad followed 48 h later by 950 rad). Four hours after the second irradiation, mice were injected with 5×10^6 bone marrow cells. After irradiation, mice were kept on drinking water fortified with sulphamethoxazole for 2 weeks to limit infection by opportunistic pathogens.

Full Methods and any associated references are available in the online version of the paper at www.nature.com/nature.

Received 3 May 2011; accepted 27 January 2012.
Published online 18 March 2012.

1. Van den Veyver, I. B. & Zoghbi, H. Y. Mutations in the gene encoding methyl-CpG-binding protein 2 cause Rett syndrome. *Brain Dev.* **23** (suppl. 1), S147–S151 (2001).

2. Van den Veyver, I. B. & Zoghbi, H. Y. Genetic basis of Rett syndrome. *Ment. Retard. Dev. Disabil. Res. Rev.* **8,** 82–86 (2002).
3. Amir, R. E. *et al.* Rett syndrome is caused by mutations in X-linked MECP2, encoding methyl-CpG-binding protein 2. *Nature Genet.* **23,** 185–188 (1999).
4. Guy, J., Hendrich, B., Holmes, M., Martin, J. E. & Bird, A. A mouse *Mecp2*-null mutation causes neurological symptoms that mimic Rett syndrome. *Nature Genet.* **27,** 322–326 (2001).
5. Nan, X. & Bird, A. The biological functions of the methyl-CpG-binding protein MeCP2 and its implication in Rett syndrome. *Brain Dev.* **23** (suppl. 1), S32–S37 (2001).
6. Luikenhuis, S., Giacometti, E., Beard, C. F. & Jaenisch, R. Expression of MeCP2 in postmitotic neurons rescues Rett syndrome in mice. *Proc. Natl Acad. Sci. USA* **101,** 6033–6038 (2004).
7. Ballas, N., Lioy, D. T., Grunseich, C. & Mandel, G. Non-cell autonomous influence of MeCP2-deficient glia on neuronal dendritic morphology. *Nature Neurosci.* **12,** 311–317 (2009).
8. Maezawa, I., Swanberg, S., Harvey, D., LaSalle, J. M. & Jin, L. W. Rett syndrome astrocytes are abnormal and spread MeCP2 deficiency through gap junctions. *J. Neurosci.* **29,** 5051–5061 (2009).
9. Lioy, D. T. *et al.* A role for glia in the progression of Rett's syndrome. *Nature* **475,** 497–500 (2011).
10. Maezawa, I. & Jin, L. W. Rett syndrome microglia damage dendrites and synapses by the elevated release of glutamate. *J. Neurosci.* **30,** 5346–5356 (2010).
11. Ginhoux, F. *et al.* Fate mapping analysis reveals that adult microglia derive from primitive macrophages. *Science* **330,** 841–845 (2010).
12. Ajami, B., Bennett, J. L., Krieger, C., Tetzlaff, W. & Rossi, F. M. Local self-renewal can sustain CNS microglia maintenance and function throughout adult life. *Nature Neurosci.* **10,** 1538–1543 (2007).
13. Mildner, A. *et al.* Microglia in the adult brain arise from Ly-6ChiCCR2^{+} monocytes only under defined host conditions. *Nature Neurosci.* **10,** 1544–1553 (2007).
14. Boissonneault, V. *et al.* Powerful beneficial effects of macrophage colony-stimulating factor on β-amyloid deposition and cognitive impairment in Alzheimer's disease. *Brain* **132,** 1078–1092 (2009).
15. Chen, S. K. *et al.* Hematopoietic origin of pathological grooming in *Hoxb8* mutant mice. *Cell* **141,** 775–785 (2010).
16. Hoogerbrugge, P. M. *et al.* Donor-derived cells in the central nervous system of twitcher mice after bone marrow transplantation. *Science* **239,** 1035–1038 (1988).
17. Simard, A. R., Soulet, D., Gowing, G., Julien, J. P. & Rivest, S. Bone marrow-derived microglia play a critical role in restricting senile plaque formation in Alzheimer's disease. *Neuron* **49,** 489–502 (2006).
18. Shechter, R. *et al.* Infiltrating blood-derived macrophages are vital cells playing an anti-inflammatory role in recovery from spinal cord injury in mice. *PLoS Med.* **6,** e1000113 (2009).
19. Chen, R. Z., Akbarian, S., Tudor, M. & Jaenisch, R. Deficiency of methyl-CpG binding protein-2 in CNS neurons results in a Rett-like phenotype in mice. *Nature Genet.* **27,** 327–331 (2001).
20. Tropea, D. *et al.* Partial reversal of Rett syndrome-like symptoms in MeCP2 mutant mice. *Proc. Natl Acad. Sci. USA* **106,** 2029–2034 (2009).
21. Willemen, H. L. *et al.* Microglial/macrophage GRK2 determines duration of peripheral IL-1β-induced hyperalgesia: contribution of spinal cord CX3CR1, p38 and IL-1 signaling. *Pain* **150,** 550–560 (2010).
22. Nijboer, C. H. *et al.* Cell-specific roles of GRK2 in onset and severity of hypoxic-ischemic brain damage in neonatal mice. *Brain Behav. Immun.* **24,** 420–426 (2010).
23. Cho, I. H. *et al.* Role of microglial IKKβ in kainic acid-induced hippocampal neuronal cell death. *Brain* **131,** 3019–3033 (2008).
24. Lu, Z. *et al.* Phagocytic activity of neuronal progenitors regulates adult neurogenesis. *Nature Cell Biol.* **13,** 1076–1083 (2011).
25. Zhang, X. *et al.* A minimally invasive, translational biomarker of ketamine-induced neuronal death in rats: microPET imaging using 18F-annexin V. *Toxicol. Sci.* **111,** 355–361 (2009).
26. Oldfors, A. *et al.* Rett syndrome: cerebellar pathology. *Pediatr. Neurol.* **6,** 310–314 (1990).
27. McGraw, C. M., Samaco, R. C. & Zoghbi, H. Y. Adult neural function requires MeCP2. *Science* **333,** 186 (2011).
28. Park, D. *et al.* BAI1 is an engulfment receptor for apoptotic cells upstream of the ELMO/Dock180/Rac module. *Nature* **450,** 430–434 (2007).
29. Guy, J., Gan, J., Selfridge, J., Cobb, S. & Bird, A. Reversal of neurological defects in a mouse model of Rett syndrome. *Science* **315,** 1143–1147 (2007).

Supplementary Information is linked to the online version of the paper at www.nature.com/nature.

Acknowledgements We thank S. Smith for editing the manuscript. We thank the members of the Kipnis laboratory as well as the members of the University of Virginia Neuroscience Department for their comments during multiple discussions of this work. We also thank S. Feldman for injection of neonatal mice, I. Smirnov for tail vein injections, and B. Tomlin and J. Jones for their animal care. N.C.D. is a recipient of a Hartwell Foundation post-doctoral fellowship. This work was primarily supported by a grant from the Rett Syndrome Research Trust (to J.K.) and in part by HD056293 and AG034113 (to J.K).

Author Contributions N.C.D. performed most of the experiments, analysed the data and prepared it for presentation, and contributed to experimental design and manuscript writing. J.C.C. performed the experiments with phagocytic activity of microglia *in vivo* and assisted with additional immunohistochemistry experiments along with data analysis and presentation, and contributed to experimental design and manuscript editing. Z.L. assisted with *in vitro* phagocytic activity experiments. E.X. assisted with animal behaviour scoring. S.B.G.A. assisted with plethysmography experiments and data analysis. P.G.G. assisted with plethysmography experimental design, data analysis and presentation of plethysmography-related data, and contributed to manuscript editing. J.K. designed the study, assisted with data analysis and presentation, and wrote the manuscript.

Author Information Reprints and permissions information is available at www.nature.com/reprints. The authors declare no competing financial interests. Readers are welcome to comment on the online version of this article at www.nature.com/nature. Correspondence and requests for materials should be addressed to J.K. (kipnis@virginia.edu).

METHODS

Animals. Male and female C57Bl/6-Tg(UBC-GFP)30Scha/J, C57Bl/6J, B6.129P2(C)Mecp2$^{tm1.1Bird}$/J, B6.129P2-Lyz2$^{tm1(cre)Ifo}$/J (*Lysm^{cre}*), B6.129P2-Mecp2^{tm2Bird}/J, *Mecp2$^{lox-stop/y}$* and C57BL/6J mice were purchased from Jackson Laboratories; B6.Cg-Mecp2$^{tm1.1Jae/Mmcd}$ mice were a gift from A. Pieper (Southwestern Medical School, Dallas, Texas, USA) and were maintained in our laboratory on C57Bl/6J background. All animals were housed in temperature and humidity controlled rooms, maintained on a 12 h/12 h light/dark cycle (lights on at 7:00) and age-matched in each experiment. All strains were kept in identical housing conditions. All procedures complied with regulations of the Institutional Animal Care and Use Committee at The University of Virginia.

Neurological assays. Mice were weighed on a laboratory scale and weights recorded to the nearest tenth of a gram; all other assays were scored on a scale from 3 to 1, with '3' being wild type (normal), and '1' being severe, as follows: gait '1', wide-spread hind limbs, severe 'waddling gait,' hopping or (unintentional) reverse locomotion; clasping '1', clenching of both rear hindlimbs tightly across ventral body aspect; tremor '1', visible involuntary shaking, particularly during or after handling; appearance '1', greasy and/or unkempt fur, clear signs of severe self-neglect in terms of grooming; kyphosis, hunched posture; eyes sunken, partly or fully closed, watery or crusted over. Scores of '2' were assigned to any phenotypes in between wild type and severe.

Bone marrow isolation. Mice were killed using CO_2 saturated with 70% alcohol. Skin was removed from the lower part of the body. Tissue was removed from hindlimbs with scissors and dissected away from body. Remaining tissue was cleaned from the tibial and femoral bones and bones were separated at the knee joint. Bone ends were cut off. Cells were forced out of bones with a stream of pH 7.4 0.1 M PBS containing 10% fetal calf serum using a 10 ml syringe with 25 gauge needle. Cells were centrifuged and re-suspended at the concentration of 2×10^7 cells per millilitre in PBS (250 µl cell suspension was injected intravenously in each animal through the tail vein).

Irradiation and bone marrow transfer. Four-week-old wild-type C57Bl/6J, B6.129P2(C)$^{Mecp2tm1.1Bird-/y}$, or B6.Cg-Mecp2$^{tm1.1Jae/Mmcd-/y}$ mice were subjected to lethal split-dose γ-irradiation (300 rad followed 48 h later by 950 rad). Four hours after the second irradiation, mice were injected with 5×10^6 bone-marrow cells freshly isolated from C57Bl/6-Tg(UBC-GFP)30Scha/J, CBySmn.CB17-Prkdc^{scid}/J or B6.Cg-Mecp2$^{tm1.1Jae/Mmcd-/y}$ mice. After irradiation, mice were kept on drinking water fortified with sulphamethoxazole for 2 weeks to limit infection by opportunistic pathogens.

Fluorescence-activated cell sorting (FACS) of brain isolates. Mice were perfused with 0.1 M PBS for 5 min. Heads were removed and skulls were quickly stripped of all flesh. Mandibles were next removed, as was all skull material rostral to maxillae. Surgical scissors (Fine Science Tools) were used to remove tops of skulls, cutting clockwise, beginning and ending inferior to the right post-tympanic hook. Brains were immediately placed in ice-cold FACS buffer (pH 7.4 0.1 M PBS, 1 mM EDTA, 1% BSA). Meninges (dura mater, arachnoid mater and pia mater) were carefully removed from the interior aspect of skulls and surfaces of brains with Dumont #5 forceps (Fine Science Tools). Brains were separated into sections (neocortex, hippocampus, striatum, cerebellum, brainstem) and sections from each group ($n = 3$ mice per group) were pooled. Brain tissue was homogenized with three gentle strokes in 10 ml FACS buffer in a 15 ml Tenbroeck Homogenizer (Lowell) then gently pressed through 70 µm nylon mesh cell strainers with sterile plastic plungers (BD Biosciences) to yield a single cell suspension. Cells were then centrifuged at 280*g* at 4 °C for 10 min, the supernatant removed and cells re-suspended in ice-cold FACS buffer. Myelin was removed using AutoMACS and myelin removal beads (Miltenyi Biotech). Cells were stained for extracellular markers with antibodies to CD11b conjugated to Alexa 780, CD45 conjugated to APC, CD4 conjugated to PE and MHC-II conjugated to Alexa 700 (eBioscience). All cells were fixed in 1% PFA in 0.1 M pH 7.4 PBS. Fluorescence data were collected with a CyAn ADP High-Performance Flow Cytometer (Dako) then analysed using Flowjo software. To obtain equivalent and accurate cell counts, cells were gated first using the LIVE/DEAD Fixable Dead Cell Stain Kit as per the manufacturer's instructions (Invitrogen), pulse width versus area to select singlet cells, forward scatter versus side scatter to eliminate debris, then by appropriate markers for cell type (for example, CD11b for myeloid-derived cells, or CD3 for T cells). Experiments were repeated twice with brains from $n = 3$ mice each group (total of $n = 6$ mice at 12 weeks after bone marrow transplantation).

Floating section immunohistochemistry. Free-floating sections were incubated with 10% normal serum (either goat or chicken) for 1 h at room temperature in PBS containing 0.1% Triton X-100 (Sigma), followed by incubation with appropriate dilutions of primary antibodies (anti-CD11b (eBioscience), 1:100; anti-MECP2 1:200 (Cell Signaling Technology); anti-cleaved caspase-3 (Cell Signaling Technology) 1:300; anti-GFP (Abcam) 1:2,000; anti-GFAP (Abcam) 1:1,000; anti-IGF-1 (R&D Systems) 1:100; anti-Lamp-1 (Abcam) 1:1000) for 24–48 h at 4 °C in the same buffer but without serum. Sections were then washed for 10 min three times at room temperature in 0.1% Triton X-100 (Sigma) in PBS followed by incubation with Alexa-fluor 488, 546, 594, 633 or 647 chicken/goat anti-mouse/rat/goat/chicken IgG antibodies (1:1,000, Invitrogen) for 1 h at room temperature. After 30 s in 1:20,000 DAPI reagent, sections were washed again with 0.1% Triton X-100 in 0.1 M PBS (3×10 min) and mounted with Aqua-Mount (Lerner Laboratories) under coverslips.

Analysis of Nissl staining. Three mice were analysed per group (wild type, *Mecp2$^{-/y}$*, wild type → wild type, wild type → *Mecp2$^{-/y}$*). Three coronal brain sections containing hippocampus were selected per mouse. Sections were incubated in 0.1% Triton X-100 (Sigma) in PBS for 10 min at 25 °C. Two washes were performed in PBS for 5 min each at 25 °C. Sections were then incubated in 1:40 Neurotrace Fluorescent Nissl Stain 530/615 Red (Molecular Probes), diluted in PBS, for 20 min at 25 °C. Sections were again incubated in 0.1% Triton X-100 (Sigma) in PBS for 10 min at 25 °C, and two washes were performed in PBS for 5 min each at 25 °C. After a final wash, sections were mounted on glass slides using Aqua-Mount (Thermo Scientific), coverslipped and visualized by confocal microscopy. Each hippocampal CA1 region (two per tissue section) was imaged, and quantified using the free hand tool in ImageJ. A Wacom computer graphics tablet was used to outline the somas of CA1 neurons, and the 'Measure and Label' function in ImageJ was used to quantify the area of each soma. After quantification, 100 soma measurements were randomly selected per mouse. This resulted in data sets of 300 soma measurements per group. GraphPad Prism was used to calculate two-way ANOVAs with Bonferonni *post-hoc* test.

Phagocytosis assay and analysis. To determine the phagocytic ability of microglial cells, we chose apoptotic neural cells as targets, because they would most closely approximate natural targets *in vivo*. Accordingly, dissociated neural progenitor cells were treated with ultraviolet light for 15 min, stained with 5(6)-TAMRA, succinimidyl ester (Invitrogen), and washed thoroughly with cold PBS before they were used for incubation with cell culture and fed on to wild-type or *Mecp2$^{-/y}$* microglial cells. After 2 or 5 hours at 37 °C and 5% CO_2, cells were removed, then washed and fixed with 4% PFA O/N. Coverslips were blocked in 10% chicken serum in 0.1 M PBS containing 0.3% Triton X-100 and 0.5% BSA, followed by incubation with anti-CD11b (eBioscience, 1:100) for 1 h at room temperature. Coverslips were then washed for 10 min three times at room temperature in 0.1% Triton X-100 (Sigma) in PBS, followed by incubation with Alexa-fluor 488 chicken anti-rat IgG antibodies (1:1,000, Invitrogen) for 1 h at room temperature. Coverslips were washed again with 0.1% Triton X-100 in 0.1 M PBS (10 min, three times) and mounted with Aqua-Mount (Lerner Laboratories) on slides. Slides were analysed using confocal microscopy and ImageJ software.

Whole-animal plethysmography. Plethysmography was performed during the dark phase of the diurnal cycle from 9:30 to 12:30 to assess normal waking respiratory parameters. Respiratory parameters were assessed by whole-animal plethysmography in unrestrained C57Bl/6J (wild-type), *Mecp2$^{-/y}$*, wild-type → *Mecp2$^{-/y}$*, *Mecp2$^{-/y}$* → *Mecp2$^{-/y}$*, wild-type → *Mecp2$^{+/-}$*, *Lysm^{cre}*, *Mecp2$^{lox-stop/y}$Lysm^{cre}* and *Mecp2$^{lox-stop/y}$* mice. Animals were placed individually into 1,000 cm^3 Plexiglas chambers (Buxco) and allowed 15 min to acclimate. The chamber was continuously flushed with dry room-temperature air (24 ± 0.5 °C) delivered by three computer-driven mass-flow regulators connected to pure O_2, N_2 and CO_2 (total flow: 1 l min^{-1}). The flow signal was recorded and analysed using EMKA IOX 2.7 (EMKA Technologies) and Spike 5.21 (CED) software. Breathing parameters were calculated from a calibrated flow signal derived from a differential pressure sensor connected to the plethysmography chamber using the equation of Drorbaugh and Fenn[30]. Real-time chamber conditions (temperature and humidity) and atmospheric pressure were continuously measured and the calculation of tidal volume was automatically adjusted to account for changes in these variables. Inspiration and expiration were detected using a pressure transducer calibrated before each experiment by injecting 1 ml of air. The pressure signal was amplified, digitized and recorded using IOX software (EMKA Technologies) and Spike2 software (Cambridge Electronic Design), concurrently. Animals were left in chambers until sufficient data representing periods of quiescent breathing were collected to allow analysis. Animals were then returned to home cages.

Analysis of plethysmography. For apnoea scoring, plethysmography traces were hand-scored for apnoeas using the following criteria: expiratory time, $T_E > 1$ s measured exclusively during periods free of grooming, sniffing or locomotor behaviour, such that false positives were excluded.

Interbreath irregularity. Interbreath variability was derived from the absolute value of $((T_{total,n} - T_{total,n+1})/T_{total,n+1})$, where $T_{total,n}$ is the duration of the breathing cycle during the *n*th breath. In each mouse this variable was determined over 100 consecutive breaths during periods when the animals were quiescent (no locomotion or sniffing) and the average value produced a single score per mouse.

This score was averaged for each group of mice and expressed as a percentage ($\pm$ s.e.m.).

Open-field activity. Behavioural testing in a novel open field was also performed during the dark phase of the diurnal cycle from 21:30 to 23:30 in the vivarium, such that measured locomotion would most closely correspond to normal waking activity. Animals were brought to the testing location within the vivarium and allowed to acclimate for 30 min before beginning the assay. Open field behaviour was measured using a Versamax activity monitor (AccuScan Instruments). Each mouse was placed initially in the centre of the monitoring cage, and allowed to roam freely for 20 min before being returned to the home cage. Animal activity levels were examined using Versamax software.

Accelerating rotarod. Motor coordination and balance were assessed on an Economex accelerating rotarod (Columbus Instruments) that had the capacity to test four mice simultaneously. The testing procedure consisted of two training phases and a testing phase: stationary training on a non-rotating rod, constant-speed training on a rod rotating at a speed of 2.0 r.p.m. and testing on an accelerating rotarod (acceleration = 0.1 r.p.m.). Latency to fall from the rotarod was recorded. For stationary training, the mouse was placed on the non-rotating rod facing the back side of the apparatus. The mouse was required to remain on the rod for 60 s before it was removed from the apparatus. If the mouse fell before the 60 s cutoff per trial, the animal was placed back onto the rod. This procedure was repeated for two trials with no inter-trial interval.For constant-speed training, the rod was adjusted to spin at a constant speed of 2.0 r.p.m. The mouse was placed on the rod facing the back side of the apparatus, and was required to remain on the rotating rod for 60 s before it was removed from the apparatus. If the mouse fell before the 60 s cutoff per trial, the animal was placed back onto the rod. This procedure was repeated for a total of two trials with no inter-trial interval. For accelerating rotarod testing, the rod was adjusted to spin at a constant speed of 2.0 r.p.m. The acceleration (acceleration = 0.1 r.p.m.) was started and the latency to fall recorded.

Microglia primary culture. Mouse mixed glia cultures were prepared from P2 mouse neonates as follows. Brains were excised and placed in ice-cold HBSS. Neocortical tissue was removed, meninges discarded and minced with forceps. Minced tissue was then incubated in 2 mg ml^{-1} papain (Sigma) in HBSS at 37 °C for 30 min. After adding cold heat-inactivated fetal bovine serum, and DNase, the tissue was washed twice with cold HBSS by re-suspending the tissue and then pelleting in a 4 °C centrifuge. To obtain a single-cell suspension, the tissue was triturated gently by pipetting through a 5 ml serological pipette 20 times and then filtered through a 70 μm nylon filter (BD Biosciences). Mixed glial cells were cultured with culture medium consisting of DMEM/F12 with 10% fetal bovine serum (Invitrogen), GlutaMAX (Invitrogen) and 1% penicillin/streptomycin in a 5% CO_2/37 °C incubator, changing medium after 7 days, for a total of 14 days. To obtain microglia, flasks were shaken at 120 r.p.m. for 12 h at 37 °C. Supernatants were collected, spun at 300*g* for 7 min, and then washed twice by re-suspending the cells in fresh medium and centrifuging at 25 °C. Cell pellets were re-suspended in culture medium and seeded at 5×10^5 cells per millilitre onto 24-well inserts (5×10^5 cells per well). Microglia were allowed to rest for 48 h before MHCII and cytokine expression assays.

Bone-marrow-derived macrophage culture. Macrophage cultures were prepared from bone marrow as follows: bone marrow was isolated as above. Five hundred thousand cells were pipetted into each well of a 24-well plate in 1 ml culture medium consisting of DMEM/F12 with 10% fetal bovine serum (Invitrogen), 10 ng ml^{-1} rMCSF (eBioscience) and 1% penicillin/streptomycin in a 5% CO_2/37 °C incubator, changing 500 μl medium after 3 days and 6 days. At 9 days, mature macrophages were washed three times with 37 °C 0.1 M PBS to remove all non-adherent cells, then placed in 1 ml culture medium consisting of DMEM/F12 with 10% fetal bovine serum (Invitrogen) and 1% penicillin/streptomycin. Cells were allowed to rest for 6 h before further treatment.

Enzyme-linked immunosorbent assay of bone-marrow-derived macrophage supernatants. Bone-marrow-derived macrophages were prepared as above. Cells were treated in triplicate wells with cytokines (50 ng ml^{-1} rIL4 or rIFNγ), or plain medium (control) and placed in a 5% CO_2/37 °C incubator for 72 h. If cells were subsequently treated with lipopolysaccharide (LPS; 100 ng ml^{-1}), they were removed from the incubator at 48 h, LPS was added and cells replaced for the final 24 h of incubation. At 72 h, 1 ml supernatant was removed from each well and frozen immediately at −80 °C. Samples were thawed simultaneously, an aliquot of each diluted 1:5 in manufacturer's diluent and enzyme-linked immunosorbent assay was performed with triplicate samples, according to the manufacturer's instructions (R&D).

TUNEL. Sections (20 μm) were sliced by cryostat and assayed the same day. Sections were permeabilized for 1 h using neuropore reagent (Trevigen) then labelled using the *In situ* Cell Death Detection Kit, Fluorescein (Roche) according to the manufacturer's instructions (using floating sections). Sections were washed 3×10 min in 0.1 M PBS, incubated for 30 s in 1:20,000 DAPI reagent, washed 1×10 min in 0.1 M PBS, mounted on slides with Aqua-Mount (Lerner) and coverslipped. Images were taken using a Zeiss LSM 700 confocal microscope. Six total slices from the cerebellum of three mice were imaged per group. Five images were taken per slice, and a randomly selected 100 μm × 100 μm section of the granular layer was sampled for each image. The area of staining was measured for each field. The staining per field was used to calculate statistics by two-way ANOVA with Bonferroni *post hoc* test using GraphPad Prism.

30. Drorbaugh, J. E. & Fenn, W. O. A barometric method for measuring ventilation in newborn infants. *Pediatrics* **16,** 81–87 (1955).